Characteristics of a SAR11 strain grown in batch and continuous culture

Scott R. Grant[a], Matthew J. Church[b], Sara Ferrón[a,c], Edward A. Laws[d], and Michael S. Rappé[e]#

[a]Department of Oceanography, School of Ocean and Earth Science and Technology, University of Hawaii at Manoa, Honolulu, Hawai'i, USA

[b]Flathead Lake Biological Station, University of Montana, Polson, Montana, USA

[c]Daniel K. Inouye Center for Microbial Oceanography: Research and Education, School of Ocean and Earth Science and Technology, University of Hawaii at Manoa, Honolulu, Hawai'i, USA

[d]Department of Environmental Sciences, College of the Coast and Environment, Louisiana State University, Baton Rouge, Louisiana, USA

[e]Hawaii Institute of Marine Biology, School of Ocean and Earth Science and Technology, University of Hawaii at Manoa, Kaneohe, Hawai'i, USA

Running Title: Growth characteristics of SAR11

#Address correspondence to Michael Rappé, rappe@hawaii.edu.

Summary word count: 250 (Abstract), 167 (Importance)

Text word count:

Abstract

In this study, a strain of SAR11 subgroup IIIa (termed HIMB114) isolated from the tropical Pacific Ocean was grown in seawater-based batch and continuous culture in order to quantify cellular features and metabolism relevant to SAR11 ecology. We report the first direct measurements of cellular elemental quotas for nitrogen (N) and phosphorus (P) for SAR11: 1.4 ± 0.9 fg N and 0.44 ± 0.01 fg P, respectively, that were consistent with the small size of HIMB114 cells (average volume of 0.09 μm^3). However, the mean carbon (C) cellular quota of 50 ± 47 fg C was anomalously high, but variable. Rates of phosphate (PO_4^{3-}) uptake measured from both batch and continuous cultures were exceptionally slow: in chemostats growing at 0.3 d^{-1}, HIMB114 took up 1.1 ± 0.3 amol P $cell^{-1}$ d^{-1}, suggesting that <30% of the cellular P requirement of HIMB114 was met by PO_4^{3-} assimilation. The mean rate of leucine incorporation, a measure of bacterial production, during late log phase growth of batch HIMB114 cultures was 0.042 ± 0.02 amol Leu $cell^{-1}$ h^{-1}. While only weakly correlated with changes in specific growth rates, the onset of stationary phase resulted in decreases in cell-specific leucine incorporation that were proportional to changes in growth rate. Rates of cellular production, respiratory oxygen consumption, and changes in total organic C concentrations constrained cellular growth efficiencies to 13 ± 4%. Hence, despite the small, streamlined genome and diminutively sized cells, SAR11 strain HIMB114 appears to grow at efficiencies similar to naturally occurring bacterioplankton communities.

Importance

While SAR11 bacteria contribute a significant fraction to the total picoplankton biomass in the ocean and likely are major players in organic C and nutrient cycling, the cellular characteristics

and metabolic features of most lineages have either been only hypothesized from genomes or otherwise not measured in controlled laboratory experimentation. The dearth of data on even the most basic characteristics for what is arguably the most abundant heterotroph in seawater has limited the specific consideration of SAR11 in ocean ecosystem modeling efforts. In this study, we provide measures of cellular P, N, C, aerobic respiration and bacterial production for a SAR11 strain growing in natural seawater media that can be used to directly relate these features of SAR11 to biogeochemical cycling in the oceans. Through the development of a chemostat system to measure nutrient uptake during steady-state growth, we have also documented inorganic P uptake rates that allude to the importance of organic phosphorous to meet cellular P demands, even in the presence of non-limiting PO_4^{3-} concentrations.

Introduction

The SAR11 bacterial lineage is a genetically diverse clade of aquatic, free-living cells with compact, streamlined genomes, found broadly distributed throughout the oceans (1). They are also among the smallest free-living cells from the ocean that have isolated strains available to study in the laboratory (2). Typical biovolumes for healthy SAR11 cells range from 0.015 to 0.058 μm^3 (3), and possess a crescent-shaped morphology (2-5). Small cells are thought to have an advantage in oligotrophic environments where they should be able to out-compete larger osmotrophs for nutrients relative to their requirements for growth, ascribed to the importance of having a large surface area to volume ratio (6).

Culture studies examining the physiology of SAR11 strains have provided a number of unexpected discoveries and valuable insights into the metabolism of the clade (1). Directed by clues generated from genome analysis indicating that a number of metabolic pathways common to chemoheterotrophs were incomplete or missing, subsequent culture studies led to evidence of unusual growth requirements for SAR11 (e.g. 5, 7-12). For example, evidence of an incomplete assimilatory sulfate reduction pathway led Tripp and colleagues to the discovery that SAR11 strain HTCC1062 requires a source of reduced sulfur for growth, which could be satisfied by methionine or dimethylsulphoniopropionate (7). Further investigations showed that SAR11 had a variant of the standard glycolysis pathways, with nonconserved ability of SAR11 strains to oxidize simple sugars, while low molecular weight organic acids were shown to be important C sources for many SAR11 strains (9). In subsequent experiments, Carini and colleagues were able to successfully grow SAR11 strain HTCC1062 on a novel defined artificial seawater medium with pyruvate serving as a source of C, methionine as a sole sulfur source, glycine as a necessary amino acid, along with standard base salts, inorganic macro-nutrients PO_4^{3-} and ammonium

81 (NH_4^+), and micro-nutrient trace metal and vitamin additions (5). Laboratory experiments with
82 isolated SAR11 strains have primarily focused on representatives from the SAR11 subclade Ia,
83 which includes the majority of isolates including '*Candidatus* Pelagibacter ubique' strain
84 HTCC1062 (2), with little information from representatives of other SAR11 subclades.

85 Recent studies suggest that the type of P available, whether present as PO_4^{3-} or dissolved
86 organic P (DOP), is an important control on microbial niche partitioning in the sea (13, 14). The
87 Global Ocean Sampling (GOS) expedition, an extensive metagenomic survey of marine surface
88 waters, revealed that genes from the high-affinity PO_4^{3-} transport system (*pstS*) most closely
89 matching sequenced *Prochlorococcus* and SAR11 genes, were among the most highly recruited
90 annotated genes (15). Moreover, during the GOS expedition, representation of *pstS* genes were
91 the single most significant difference between the tropical Atlantic and equatorial Pacific
92 samples, varying by a factor of more than seven in relative abundance (15). Studies of culture
93 representatives of *Prochlorococcus*, the most abundant oxygenic photoautotroph in the ocean,
94 confirm that there appear to be substantial differences in the presence, topology, and regulation
95 of genes thought to be involved in P acquisition between strains of *Prochlorococcus* (16), with
96 different strains able to metabolize inorganic vs. labile organic P compounds. Finally, in a gene
97 content comparison of whole population genomes of *Prochlorococcus* and SAR11 between
98 microbial communities inhabiting the well-known stations of the Hawaii Ocean Time-series
99 (HOT) program (North Pacific) and the Bermuda Atlantic Time-series Study (BATS) (North
100 Atlantic), Coleman and Chisholm found that of the 1.8% of gene clusters which had significant
101 abundance differences between the Atlantic and Pacific populations, 87% of those genes were
102 involved in PO_4^{3-} or phosphonate metabolism (17).

103 Motivated by the intriguing evidence that P acquisition strategies are under strong
104 selection pressure and may be a potential dimension over which SAR11 lineages are
105 differentiated, this study sought to investigate the uptake capability of the SAR11 subclade IIIa
106 isolate HIMB114 for PO_4^{3-}. Because SAR11 bacteria characteristically dominate marine
107 planktonic microbial communities, it is also a notable deficiency that typical parameters needed
108 to model their growth and response under variable environmental conditions are not yet
109 available. Thus, this study also sought to measure a number of basic cellular properties such as
110 elemental composition, and physiological rate measurements including cellular production,
111 respiration, and growth efficiency. In the process, a continuous culture of an axenic SAR11
112 strain was developed for the first time, enabling assessment of many of these physiological
113 features under defined growth conditions.
114

Results

Culture growth and cell size. In natural seawater-based growth media, strain HIMB114 reached a maximum specific growth rate of 1.2 d^{-1} and yielded 5-8 $\times 10^5$ cells mL^{-1} (Fig. S1). HIMB114 cells were observed to have a crescent-shaped morphology that was consistent with previous microscopic observations of SAR11 (Fig. 1). Elongated cells of HIMB114 were observed that consisted of spirillum morphologies of two to four "regular" (i.e. recently divided) single-cell lengths. These longer cell morphologies were a small fraction (few percent) of the cells during exponential growth phase, but became an increasing percentage (up to 30%) of cells as the culture entered into stationary phase. Distributions of cell size parameters for length, width, and biovolume were all non-normal and fit as log-normal distributions to calculate the most frequent and mean size parameter values (Fig. S2). The mean of the distribution was used when normalizing any quantities to a cell size parameter (length 1.07 µm; width 0.32 µm; volume 0.09 μm^3).

Cellular elemental quotas. The P cell quota for HIMB114 measured for batch cultures in early stationary phase was 14.2 ± 0.4 amol P $cell^{-1}$ (mean ± s.d.; n=6) or 0.44 fg P $cell^{-1}$, with a mean precision of 2% for triplicate 4–5 L culture volumes. The particulate P controls made from spent media were 5% of that measured for the cellular biomass collected on their corresponding 0.2 µm pore-sized membrane filter. Hence, the modified method for measuring particulate P on 47 mm diameter PC membranes described in the Materials and Methods appeared to work well.

Filtered media blanks for particulate C and N were high relative to the sample signal, and increased with the volume of media filtered (Fig. S3). Because complete saturation was not conclusive even at a media blank volume of 10 L, rectangular hyperbolic saturation functions

were fit by non-linear least squares regression to the blank C and N data versus filtered media volume in order to extrapolate the associated blank values for the 30 L of total volume filtered (Fig. S3). After normalizing to the total number of cells captured on each filter, the mean C cell quota was 50 ± 47 fg C $cell^{-1}$ (mean ± s.d.; n=3) or 4.2 fmol C $cell^{-1}$, and the mean N cell quota was 1.4 ± 0.9 fg N $cell^{-1}$ (mean ± s.d.; n=3) or 0.1 fmol N $cell^{-1}$.

PO_4^{3-} uptake in batch and continuous culture. Rates of PO_4^{3-} uptake measured by ^{33}P-radiotracer for a continuous culture of HIMB114 were extremely slow (Fig. 2A). Of the five PO_4^{3-} uptake rate time course measurements performed from the chemostat cultures over 4 to 6 h at ambient (100 nmol L^{-1}) phosphate concentrations, the mean specific uptake rate was 0.007 ± 0.0025 d^{-1} (mean ± s.d.; n=5), with a mean coefficient of determination of uptake vs. time of 0.97 (Fig. 2A). This corresponds to a mean PO_4^{3-} turnover time (T_P) of 160 ± 50 days (mean ± s.d.; n=5), or a bulk PO_4^{3-} uptake rate of 0.68 nmol L^{-1} P d^{-1}. In cell specific units, HIMB114 took up 1.1 ± 0.3 amol P $cell^{-1}$ d^{-1} (mean ± s.d.; n=5), or less than 10% of the cellular P quota per day, despite growing at a rate of 0.3 d^{-1}. Phosphate uptake kinetics measured for the chemostat culture averaged 0.4 ± 0.09 nmol L^{-1} P d^{-1} (mean ± s.d.; n=9) across all PO_4^{3-} additions, showing no significant correlation between uptake rate and PO_4^{3-} concentration within the error of the measurements (Fig. 2B). This observation most likely reflects the fact that the culture was not P-limited; an interpretation confirmed by the fact that PO_4^{3-} additions to batch cultures entering stationary phase had no affect on growth (not shown).

For HIMB114 grown under batch conditions, PO_4^{3-} uptake rates were also extremely low (Fig. 2A). Measured during late exponential phase for a culture growing at 1.02 d^{-1}, the highest specific uptake rate measured was 4×10^{-5} d^{-1}, equivalent to a turnover time of the PO_4^{3-} pool of

161 70 years (ranging 50 to 100 years). In bulk units, the maximum PO_4^{3-} uptake rate for the batch
162 cultures in late exponential growth was 6 pmol P L^{-1} d^{-1}. To confirm that the cells were actively
163 growing, leucine incorporation measurements were conducted at the same time as the PO_4^{3-}
164 uptake measurements (described in greater detail below). The resulting production rate was 37 ±
165 2.6 nmol C L^{-1} d^{-1} (mean ± s.d.; n=4) that, when converted to P units using a 50:1 C:P molar
166 ratio, yields a P requirement of 0.7 nmol P L^{-1} d^{-1}. Given that the measured bulk PO_4^{3-} uptake
167 rate was 6 pmol P L^{-1} d^{-1} (or ~1% of the requirement), such results suggest PO_4^{3-} was not the
168 primary source of P for HIMB114 growing on natural seawater based media containing 100-150
169 nmol PO_4 L^{-1}.
170
171 **Chemostat steady-state theory.** The theoretical expectations for PO_4^{3-} uptake rate and turnover
172 time measurements for the chemostat system are fairly well constrained, much better than for
173 batch culture growth, because steady state theory may be applied (18). The cell specific uptake
174 rate is the product of the specific growth rate (μ) with the cellular P quota (Q_P):

175 $$V = \mu \cdot Q_P$$

176 The growth rate is experimentally set by the chemostat dilution rate, here 0.3 d^{-1}. The cellular P-
177 quota (measured at 14.2 amol P $cell^{-1}$) yielded a theoretical uptake rate of 4.3 ± 0.5 amol P $cell^{-1}$
178 d^{-1}. In comparison, the highest measured uptake rate was 1.3 ± 0.2 amol P $cell^{-1}$ d^{-1}, or about
179 30% of the theoretical value. This was the highest uptake rate measured for the culture and,
180 consistent with results from the batch culture, indicated that HIMB114 growing under steady-
181 state conditions with PO_4^{3-} concentrations at 100 nmol L^{-1} was likely not using PO_4^{3-} as a sole or
182 primary P source for growth, and was instead meeting a large fraction of its P requirements from
183 assimilation of organic P.

Bacterial production. Bacterial production measurements were conducted on four consecutive days spanning the end of log phase into the early transition to stationary phase from the five batch culture experiments (Fig. 3A, Fig. S4). The mean per cell rate of leucine incorporation across all cultures grown on K-Bay standard medium was 0.042 ± 0.02 amol Leu $cell^{-1}$ h^{-1} (mean ± s.d.; n=20), resulting in average cell-specific rates of production of 0.13 ± 0.07 fmol C $cell^{-1}$ d^{-1} (mean ± s.d.; n=20) (Table 1).

Bacterial production measurements for HIMB114 were relatively uniform, with a coefficient of variation of 40% across the 10 different cultures and 20 independent measurements grown on natural K-Bay seawater medium, despite being measured across a range of growth rates throughout exponential and early stationary phases of batch growth (linear correlation coefficient of 0.58, p-value 0.009) (Fig. 3B). However, in individual batch culture experiments, a decline in rate of cell division associated with entry into stationary phase was associated with a concomitant decline in production measured by leucine incorporation (Fig. 3A, Fig. S4), and the slope of the fit line for the plot of bacterial production vs. specific growth rate was positive (0.8 ± 0.3 (95% C.I.) $\times 10^6$ molecules Leu $cell^{-1}$).

Respiration. Rates of respiration were determined from three incubation experiments subsampled from the batch cultures (Table 2). Respiration was derived from linear regression fits to time course experiments in which the concentration of O_2 was measured over two-day incubation periods (Figs. 3A and 4). Although extensive measures were taken to thoroughly acid clean and rinse the glass bottles, HIMB114 cells were only able to grow in the glass incubation bottles for a period of about two days and the consumption of O_2 was only linear over this initial

~two-day period (Fig. 4). Respiration rates showed high reproducibility over the three incubation experiments [0.37 ± 0.06 µmol O_2 L^{-1} d^{-1} (mean ± s.d., n=3)] (Table 2) for cultures beginning with cell densities near 2 × 10^5 mL^{-1} at the start of the incubations, and increasing on average 2.5 times over the two-day incubation period to about 5 × 10^5 mL^{-1}. Cell-normalized rates of respiration averaged ~1 fmol O_2 $cell^{-1}$ d^{-1} when cultures were transitioning from exponential growth to stationary phase at a specific growth rate of approximately 0.5 d^{-1}.

Rates of respiration were also derived based on changes in total organic C (TOC) within HIMB114 cultures over several days, measured at the start and end of the incubations of six replicate 10 L batch cultures of HIMB114 (Fig. S1). The initial TOC concentration in the media was 83 ± 2 µmol C L^{-1} (mean ± s.d., n=6), while the final TOC concentration sampled 9 days later was 79 ± 3 µmol C L^{-1} (mean ± s.d., n=6), resulting in a mean drawdown of TOC over the 9-day incubation of 4 ± 4 µmol C L^{-1} (mean ± s.d., n=6). This is equivalent to approximately 5% of initial TOC. The resulting average rate of respiration was 0.44 ± 0.44 µmol C L^{-1} d^{-1}. This rate is very similar to the mean rate of O_2 consumption (based on the two day incubation period), assuming a respiratory quotient of 1 mol C: mol O_2, of 0.37 ± 0.06 µmol C L^{-1} d^{-1} (mean ± s.d., n=3).

Bacterial growth efficiency. By combining rates of bacterial production with the measured rates of respiration we were able to estimate bacterial growth efficiency (BGE) for the HIMB114 batch cultures. BGE is defined as the ratio of the C production rate to the total C demand, which is the sum of production and respiration:

$$BGE = \frac{BP}{BP + BR}$$

Combining these rate measurements resulted in a mean BGE of 13% with a 95% confidence interval of 10 – 21% estimated by a Monte Carlo simulation study (Table 2).

Discussion

Steady state chemostat growth provides an ideal system to investigate the physiology and cellular properties of model microorganisms. The chemostat system allows the investigation of cellular physiology under controlled growth rate conditions, something unachievable using batch cultures. In this case, the steady state growth achieved through the chemostat allowed us to simultaneously calculate the theoretical P demand as well as determine the actual PO_4^{3-} uptake rate at a set rate of growth. Despite the inability to grow strain HIMB114 under P-limiting conditions, these experiments suggest that this isolate relies heavily on sources of P other than PO_4^{3-} when grown on a natural seawater minimal medium. This finding is particularly intriguing considering that HIMB114 has a complete high-affinity PO_4^{3-} transport system (19), and so should have the full capacity to transport PO_4^{3-} under dilute conditions. While inorganic PO_4^{3-} is generally considered the preferred P source for marine bacteria (14), oligotrophic marine environments such as Kaneohe Bay in the tropical Pacific Ocean where strain HIMB114 was isolated typically have DOP concentrations an order of magnitude above inorganic phosphate concentrations (20). Thus, the ability to utilize components of the DOP pool to attain P may be competitively advantageous. In both batch and chemostat culture conditions, HIMB114 appeared to utilize an undetermined component of the DOP pool to meet its P growth demands, even when PO_4^{3-} was amended to the media. Which component(s) of the DOP pool were utilized remains to be determined. One potential class of DOP compounds receiving recent attention are phosphonates, which are organic phosphonic acid derivatives containing a C-P bond and which

make up 25% of the high molecular weight DOM pool (21). Evidence of the widespread distribution of genes for the transport and metabolism of phosphonates has been reported in marine microorganisms (22-24) including SAR11 (Table S1) (17, 19), and there is precedent for the PO_4^{3-}-independent utilization of phosphonates in marine systems (25). In laboratory experiments with a defined growth medium, SAR11 subgroup Ia strain HTCC7211 was shown to utilize phosphonates as a source of P for growth (12). While the genome of strain HIMB114 encodes for a complete phosphonate transport system similar to that of HTCC7211, it encodes a unique and sparse complement of genes for phosphonate metabolism (Table S1).

At 14.2 amol P cell^{-1}, the measured P cell quota for HIMB114 is close to that determined for SAR11 subgroup Ia strain HTCC7211 (10.9 amol P cell^{-1}) grown on a P-limiting, defined medium (12). Using transmission electron microscopy coupled with X-ray microanalysis, Gundersen and colleagues found an empirical biovolume (V) power law relationship for cell P quotas of $126V^{0.937}$ amol P cell^{-1}, measured for 84 bacterial cells with mean cell volume 0.08 µm^3 (range 0.001 to 2.0 µm^3) (26). Using this power law for HIMB114 cells suggests a cellular quota of 13 amol P cell^{-1}, similar to the value measured in our study. At 1.237 Mbp and 2 P-atoms per base pair, the small genome of HIMB114 yields a P content of 4.1 amol P cell^{-1}. This calculation suggests DNA alone accounts for approximately 29% of the cellular P-quota, a finding roughly 2 to 3 times the 10-15% cellular P traditionally considered accounted for by DNA in a bacterial cell (27). Another significant pool for P is likely phospholipids, which have previously been measured to contain 2.5 amol P cell^{-1} for strain HIMB114 grown in PO_4^{3-} replete seawater media (28). Thus, nearly half of the P-quota of the cell can be accounted for by only two macro-molecular components: DNA and phospholipids. While not quantified in HIMB114 or other SAR11 cultures, RNA is typically the dominant contributing molecular pool

to cellular P; typical total RNA to DNA mass ratios are infrequently below 2:1 (mass RNA: mass DNA), even for slowly growing bacteria (29). At a lower limit of 1:1 RNA:DNA, an additional 4.1 amol P $cell^{-1}$ can be accounted for by inclusion of cellular RNA pools. Hence, HIMB114 appears to have a similar cellular P concentration (0.16 M P) compared to other marine bacteria (0.1 to 0.2 M P) (30), and it would be difficult to further reduce this P demand unless these cells were able to substitute P-free lipids for phospholipids as has been demonstrated for SAR11 subgroup Ia strain HTCC7211 (31). However, no genetic capacity for phospholipid substitution analogous to that found in the genome of strain HTCC7211 is apparent in the HIMB114 genome.

At 0.05 μm^3, the peak of the distribution for cell volume of strain HIMB114 was consistent with the recently reported range of 0.015 to 0.058 μm^3 for SAR11 subclade Ia isolates HTCC1062 and HTCC7211 (3). However, the mean value of the cell volume distribution (0.09 μm^3) for HIMB114 was larger than anticipated, which can be at least partially attributed to elongated and chains of cells that increase in frequency as HIMB114 enters into stationary phase (Fig. 1). This phenomenon has been observed previously for SAR11 subgroup Ia strain HTCC1062 (5) and thus may be a broadly distributed, growth stage-dependent feature of SAR11 that has the potential to confound models and other measurements that rely on an average cell size or that are normalized per cell. For example, this phenomenon may contribute to the variability observed between bacterial production measured by leucine incorporation and cellular growth rate during the transition to stationary phase (Fig. 3).

The genome and the membrane envelope are two essential components of a cell that cannot be continuously scaled down with cell size (6), and hence represent increasing fractions of total cell volume, or mass, for cell volumes below 0.05 μm^3 (Fig. S5). This constrains the lower limit for a bacterial cell volume to about 0.004 μm^3. We therefore propose a potential

297 trade-off between nutrient acquisition strategies and P growth requirements for small cells. In
298 oligotrophic, nutrient-limited environments, a high surface area to volume ratio should increase a
299 cells ability to compete for dilute nutrients, giving small cells a distinct competitive advantage.
300 Yet, there is an opposing force balancing this trend toward smaller cell size, namely an
301 increasing P requirement relative to cell mass necessary to maintain a given growth rate. This
302 trade-off is reflected in the importance of P-sparing strategies employed by oligotrophic
303 picocyanobacteria such as *Prochlorococcus* (32), and the noted prevalence and diversity of P
304 acquisition and metabolism related genes found to be important across large ocean ecosystem
305 regimes (15, 17). In addition to membrane lipid renovation (31), strategies employed by very
306 small, diverse, and successful bacteria of the SAR11 clade to sustain cellular P demands and
307 otherwise maintain sufficient net growth rates to numerically dominate surface marine waters
308 will no doubt continue to provide interesting discoveries.

309 The exceedingly high C to N stoichiometry of near 40±14:1 (mol C: mol N) is well
310 outside normally reported ranges for bulk marine particulate organic matter or C:N ratios of flow
311 cytometrically sorted natural planktonic populations (max 24.4, mean 9.4±3.6, n=277) (33).
312 Moreover, the resulting C: N: P cellular stoichiometry for HIMB114 would approach 300:7:1
313 (mol C : mol N : mol P), a finding inconsistent with previous estimates for members of the
314 SAR11 clade. Such results are primarily driven by the exceedingly large C cell quota measured
315 for HIMB114 in this study (50 ± 47 fg). The N cell quota for HIMB114 (1.4 ± 0.9 fg) is slightly
316 lower than the minimum N cell quota of 1.6 fg N for natural bacteria reported by Fagerbakke,
317 Heldal & Norland, (30). Using the biovolume power law regression from Gundersen et al., (26)
318 to derive cellular N quotas results in 2.4 fg N for a cell volume of 0.09 μm^3 (mean volume
319 measured in the current study); the same relationship yields a cellular C quota of ~13 fg C. Tripp

and colleagues previously estimated that SAR11 subgroup Ia strain HTCC1062 contained 5.8 fg C $cell^{-1}$ for cells of biovolume 0.035 μm^{-3} (7), which scales to 14.9 fg C $cell^{-1}$ for a cellular volume of 0.09 μm^3. Similarly, Cermak and colleagues estimated that cellular C quotas varied between 12 to 16 fg for SAR11 strains HTCC1062 and HTCC7211 (34), which would scale to 24 to 48 fg C for HIMB114 when accounting for differences in cell volume. Such comparisons suggest the measurements of cellular C from the current study are overestimates. Although it remains unclear what factors may have contributed to these results, such findings may reflect the poor filtration retention efficiency of the filters utilized for these measurements. Regardless, accurate quantification of cellular C content of SAR11 cells remains imperative for future research efforts.

Although there are no published bacterial production measurements for any axenic SAR11 cultures, we can compare our values to measurements from planktonic marine ecosystems where SAR11 often dominate. The observed mean leucine incorporation rate from this study (4.2×10^{-8} pmol Leu $cell^{-1}$ h^{-1}) is very close to that of the natural community mean dark leucine incorporation rates, normalized to non-pigmented cell counts, for station ALOHA in the North Pacific subtropical gyre of 5×10^{-8} pmol Leu $cell^{-1}$ h^{-1} (35), and falls at the lower end of the range measured for natural surface seawater communities along a transect off the Oregon coast ($0.39–4.7 \times 10^{-7}$ pmol Leu $cell^{-1}$ h^{-1}) (36). Malmstrom and colleagues measured the contribution of naturally occurring SAR11 populations to bulk ^{3}H-leucine incorporation rates using a combination of microautoradiography and fluorescence *in situ* hybridization (Micro-FISH) in the Northwest Atlantic Ocean (37). These authors reported that SAR11 accounted for a large fraction (50%) of the bulk leucine incorporation rates in surface waters, where they represented 25–35% ($2–4 \times 10^8$ cells L^{-1}) of the picoplankton population. The resulting SAR11-

specific C production rates were estimated to be from 0.5 µg C L^{-1} d^{-1} for an open-ocean Gulf Stream site, increasing to about 3 µg C L^{-1} d^{-1} for a coastal location. del Giorgio and Cole compiled published marine ecosystem bacterial production measurements and reported global mean bacterial production rates of 2.41 ± 0.33 µg C L^{-1} d^{-1} for the coastal ocean to 0.37 ± 0.054 µg C L^{-1} d^{-1} for the open ocean (38). In the current study, the bulk C production rate measured for HIMB114 cultures was 0.6 ± 0.2 µg C L^{-1} d^{-1}, similar to those estimated by Malmstrom and colleagues (37) and typical of open-ocean, oligotrophic values reported by del Giorgio and Cole (38).

Leucine incorporation rates are used as a standard proxy for biomass production under the assumption that protein is a major constituent of cell biomass, and that leucine represents a relatively stable proportion of bacterial protein (39). This allows consistent comparisons of protein synthesis rates, and thus biomass production, across the wide spectrum of bacterial species capable of taking up leucine. It was somewhat surprising then to find that bacterial production measured by leucine incorporation varied little across a range of growth rates for HIMB114, with only a weak correlation between the two measures. While this could be due to the low precision (typically 15%) for both cell counts and leucine incorporation measures, it is also possible that protein production rates and cell division rates are uncoupled at short time scales under non-linear batch growth.

We also measured O_2-based rates of respiration, with rates averaging ~0.4 µmol O_2 L^{-1} d^{-1}. These low rates of respiration were highly reproducible, with a coefficient of variation of 16% between replicate incubations. Moreover, the measured O_2-based respiration measurements agreed with the measured drawdown of organic carbon over the course of the incubations, which together with measured rates of bacterial production yielded estimates of BGE near 13%. Such

366 results suggest HIMB114 grows at similar efficiencies as other marine heterotrophic bacteria,
367 despite features such as an exceptionally small, streamlined genome that might be expected to
368 enable more efficient growth.

369 Steindler and colleagues have published the only other dissolved oxygen measurements
370 from a SAR11 culture, wherein SAR11 subgroup Ia strain HTCC1062 cultures were measured
371 using an oxygen optode (4). Although rates of respiration were not explicitly calculated in that
372 study, over the initial 69 h period of incubation concentrations of O_2 declined by approximately
373 100 μmol O_2 L^{-1}, equivalent to a rate of O_2 consumption of ~35 μmol O_2 L^{-1} d^{-1}. Cell densities
374 in the experiments of Steindler and colleagues were three orders of magnitude higher than the
375 densities of our experiment; when normalized to cell density, the rate of respiration for
376 HTCC1062 was approximately 0.35 fmol O_2 $cell^{-1}$ d^{-1}, approximately one third of the rate
377 observed for strain HIMB114.
378

379 **Conclusions**

380 Though we were unable to create a state of P-limited growth or to determine what may be
381 limiting HIMB114 when grown on a minimal seawater medium, we were able to rule out many
382 of the common C, sulfur, and specific amino acid growth substrates that have been shown to
383 enhance growth for other SAR11 cultures and permit their growth in a defined, artificial
384 seawater growth medium (5, 7, 8, 11, 40). While this implies caution in extrapolating the results
385 of culture-based studies from specific SAR11 isolates to the SAR11 lineage as a whole, it also
386 suggests that exciting metabolic features that distinguish populations, ecotypes, and major
387 SAR11 sub-lineages await characterization. One such feature, uncovered by using a continuous
388 culture of HIMB114, is the apparent inability of this strain to fulfill its cellular P-demand

through the uptake of PO_4^{3-} alone. Our findings support the idea that at least some members of the SAR11 clade rely on organic P to support growth, which is also supplemented by the use of cellular P-sparing adaptations such as lipid renovation (1). Despite potential methodological issues with the measurement of cellular C content, the N and P cell quotas, production, respiration, and cell size measurements reported here provide new information for scientists and modelers interested in understanding the impact of SAR11 cells on the ecology of the global ocean.

Materials & Methods

SAR11 strain HIMB114 was previously isolated from Kaneohe Bay on the northeastern shore of the island of Oahu in the tropical Pacific Ocean using a dilution-to-extinction approach (2, 41). It is a member of subclade IIIa that, based on genome comparisons, exhibits genus-level divergence from the comparatively well-studied members of subgroup Ia (i.e. '*Candidatus* Pelagibacter') (19, 42, 43). HIMB114 would not grow in defined artificial seawater-based media previously published for SAR11 (5, 40), nor could we enhance its cellular yield by previous organic carbon, vitamin, and nutrient additions that have proven successful for other SAR11 strains (7, 8, 11) (data not shown). Thus, all experiments were performed in natural seawater-based minimal media with seawater collected from the southern basin of Kaneohe Bay (21º 26.181' N, 157º 46.642' W). To make growth media, 200 L of surface seawater was filtered through pre-rinsed (10 L sterile water followed by 10 L seawater) 0.1 µm pore-sized polyethersulfone (PES) membranes (AcroPak 1000; Pall Corp., Port Washington, NY, USA) into clean 10 L polycarbonate (PC) carboys. Individual 10 L batches of seawater were subsequently autoclaved for 2.5 hours (h) at 121 °C and allowed to cool. For both batch and chemostat media (media termed "K-Bay"), the seawater base was amended with nitrate (3 µmol L^{-1} $NaNO_3$), NH_4^+ (3 µmol L^{-1} NH_4Cl), PO_4^{3-} (0.1 µmol L^{-1} KH_2PO_4), and a vitamin stock solution added at 10^{-5} dilution (10^{-6} dilution for the chemostat medium) (2). All chemicals were BioUltra grade (MilliporeSigma, St. Louis, MO, USA). The vitamin stock solution contained B1 (thiamine hyrdochloride, 1 g L^{-1}); B3 (niacin, 0.1 g L^{-1}), B5 (pantothenic acid, 0.2 g L^{-1}); B6 (pyridoxine, 0.1 g L^{-1}); B7 (biotin, 1 mg L^{-1}); B9 (folic acid, 2 mg L^{-1}); B12 (cyanocobalamin, 1 mg L^{-1}); myo-inositol (1 g L^{-1}); and PABA (4-aminobenzoic acid, 0.1 g L^{-1}). Following nutrient additions, small amounts of autoclaved-sterile milli-Q deionized-water was added to the K-Bay

media to replace water lost as a result of autoclaving, achieving a final salinity of 32. The media were then sparged with CO_2, followed by air, through three in-line Whatman (GE Healthcare Life Sciences, Chicago, IL, USA) vent filters (HEPA 0.3 µm glass fiber to 0.2 µm PTFE to 0.1 µm PTFE) to restore the inorganic C chemistry and to bring the media pH to between 8.0 and 8.1, and stored at 4 °C until use. HIMB114 cultures were grown in batch at 26 °C under low light (33 µmol quanta m^{-2} s^{-1}) and a 12/12 light/dark cycle in volumes ranging from 100 mL to 10 L, as well as a 4 L continuous culture chemostat system (described below).

Chemostat. For continuous culture growth, a custom-built 4 L PC chemostat was constructed using a narrow mouth 4 L PC bottle, 4-port Teflon threaded cap, PC Luer connection fittings, and silicone tubing for the inflow of growth medium, culture overflow, air bubbling, and culture sampling ports. The chemostat was kept under positive pressure by bubbling with 0.1 µm-filtered air, which served to keep the culture well-mixed as well as provide positive pressure for culture sampling. Media was pumped from a 10 L PC carboy continuously at 0.85 mL min^{-1} for a target dilution rate of 0.3 d^{-1}. Overflow was continuously removed into a PC bottle used as an overflow container. To start the continuously growing culture, the chemostat was filled to 2 L with the K-Bay chemostat medium (Table 2), inoculated with 5 mL of a growing HIMB114 culture, and allowed to grow in batch, where it reached an exponential growth rate of 0.75 d^{-1} for 10 days before media in-flow was started (Fig. 5). After reaching the full 4 L chemostat volume, cell densities stabilized at 7×10^5 mL^{-1} after approximately 5 days, and remained in continuous culture for 12 days or about 5 doubling times with continuous media inflow and culture overflow (Fig. 5). The culture was grown in the chemostat for a total of 40 days; however, following the connection of the third 10 L batch of new K-Bay chemostat medium at day 30, cell densities

444 slowly declined to 3.5×10^5 mL^{-1} by the end of the 40 days when the chemostat was turned off
445 (Fig. 5).
446
447 **Cell enumeration and image analysis.** Culture cell counts were made by 4',6-diamidino-2-
448 phenylindole (DAPI) staining and subsequent epifluorescence microscopy. Depending on culture
449 density, between 2 to 10 mL culture samples were fixed with 20% electron microscopy grade
450 paraformaldehyde solution (Electron Microscopy Sciences, Hatfield, PA, USA) to a final fixative
451 concentration of 0.4%, and stored at 4 °C overnight. DAPI was subsequently added to a final
452 concentration of 5 μg L^{-1} and incubated in the dark at room temperature for at least 20 minutes.
453 Stained samples were filtered onto 25 mm diameter, 0.2 μm pore-sized, black Nuclepore (GE
454 Healthcare Life Sciences) or Isopore (MilliporeSigma) PC membranes, with a 0.8 μm pore-sized
455 GN-4 (Pall Corp.) mixed cellulose ester backing filter. Filters were allowed to air dry for 15
456 minutes and either stored frozen (-20 °C) or mounted in high-viscosity immersion oil on a glass
457 slide for microscopic enumeration. At the volumes filtered, the precision of epifluorescence
458 microscope cell counts were between 10% to 20% for densities above 10^4 mL^{-1}. Cell number
459 and size information (including cell lengths and widths) were calculated by image detection
460 software from DAPI stained epifluorescence images captured with a Retiga EXi FAST1394
461 camera (QImaging, Surrey, BC, Canada) at 1000x magnification.
462 Cell morphology was also visualized via scanning electron microscopy. HIMB114 cells
463 grown in K-bay media to early stationary phase were fixed with gluteraldehyde (20%; Electron
464 Microscopy Sciences), filtered onto 0.2 μm pore-sized PC membranes (Nuclepore), washed with
465 sodium cacodyolate buffer, post-fixed in osmium tetraoxide, and subjected to sequential ethanol
466 dehydration, critical point drying with CO_2, and coating with gold/palladium. The preps were

viewed on a Hitachi S-4800 Field Emission Scanning Electron Microscope with Oxford INCA X-Act EDS System.

PO_4^{3-} uptake. Rates of PO_4^{3-} uptake were measured in both batch and continuous culture using ^{33}P-radiotracer methods (18). In brief, between 10–50 mL aliquots of growing culture were sampled into 50 mL PC tubes and spiked with ^{33}P-orthophosphoric acid (158 Ci mg^{-1}; PerkinElmer, Waltham, MA, USA) to a specific activity of 50 µCi L^{-1}. ^{33}P-labeled cultures were incubated (typically for 4 to 8 h) under identical growth conditions to the parent cultures. Sample time points were collected by low-vacuum filtration of 5 mL onto 0.2 µm pore-sized, 25 mm diameter PC Nuclepore membranes, each filter having been pre-saturated with unlabeled PO_4^{3-} by the addition of 1 mL of high PO_4^{3-} (0.1 mmol L^{-1} PO_4) seawater to each filter prior to sampling (Suppl. Info.). Following filtration of ^{33}P-labeled samples, filters were rinsed with 10 mL of 0.2 µm-filtered seawater. Along with the culture samples, 0.2 µm-filtered seawater controls amended with ^{33}P-radiotracer served as non-biological blanks; these blanks were incubated and processed identical to samples. Phosphate uptake kinetics were also conducted for nine treatments of increasing PO_4^{3-} concentration by the addition of 1 – 20 µL of concentrated unlabeled phosphate stocks (0.1 – 1 mmol L^{-1} KH_2PO_4) to 11 mL chemostat culture samples. The treatments and filtered seawater controls were subsampled (2 mL) at 5 time points over 22 hours of batch growth.

Bacterial production. Bacterial production was estimated based on the incorporation of tritiated-leucine (^{3}H-Leu) into protein using small volume (1.5 mL) sample incubations based on

the microcentrifugation method (44) (Suppl. Info.). Leucine incorporation rates were converted into C production rates using a standard 1.5 kg C mol Leu^{-1} conversion factor (36).

Oxygen respiration. Respiration rates were measured in batch cultures of strain HIMB114 based on time-dependent changes in oxygen to argon (O_2/Ar) ratios measured by membrane inlet mass spectrometry (MIMS) (45) (Suppl. Info.). Cultures growing in late exponential phase in 10 L PC carboys were siphoned using silicone tubing into 70 mL clear glass serum bottles, allowed to overflow, capped with Teflon lined rubber stoppers, and crimped sealed. The glass bottles were extensively cleaned with milli-Q DI-water and 10% hydrochloric acid, and finally autoclaved while filled with milli-Q DI-water before use. Sample bottles were filled in triplicate for each time point, with 5 time points sampled over a two-day period, and in one case a four-day period. Bottles were incubated under the same temperature and light conditions as the original cultures, and either run immediately at each time point or killed by syringe addition of 100 µL of saturated mercuric chloride solution and analyzed at the end of the incubations.

Monte Carlo simulation. A Monte Carlo simulation study was conducted to quantify statistical errors in the oxygen-based respiration, bacterial production, and BGE measurements. Simulated data for O_2 concentrations and leucine incorporation rates from the respiration and production experiments were generated by sampling (N=10,000) from independent, normal distributions using sample means and variances based on experimental replicate measurements. Linear regression slopes were computed on the simulated O_2 concentration samples with time to obtain simulated O_2 respiration rates separately for each of three incubation experiments, with regression slopes bounded by zero (i.e., simulated data was prevented from indicating net O_2

512 production with time). To convert from O_2 and leucine units into carbon units, no uncertainty
513 was assumed in the conversion factors, as we were attempting to estimate the statistical error
514 from our measurement replication. BGE was calculated as indicated above, and 95% confidence
515 intervals (2.5% and 97.5% quantiles) were calculated for each measurement by experiment
516 (Table 2) and for the final reported mean BGE measure.
517
518 **Dissolved nutrients.** Samples for dissolved inorganic nutrients and TOC analyses were taken
519 from both the original medium as well as the final spent medium at the end of culture
520 incubations. Samples were collected in acid washed, DI-water rinsed plastic (inorganic nutrients)
521 or glass (TOC) containers, and stored frozen until analysis. Dissolved inorganic nutrient samples
522 were analyzed on a Analytical Segmented Flow Injection AutoAnalyzer AA3 HR (SEAL
523 Analytical Inc., Mequon, WI) for the determination of PO_4^{3-}, NH_4^+, nitrate + nitrite (NO_3^- +
524 NO_2^-), silicate (SiO_4), and total N. Samples for TOC were acidified and O_2 purged to remove
525 inorganic C, and measured using high temperature catalytic oxidation on a Shimadzu TOC-L
526 (Schimadzu Scientific Instruments Inc., Columbia, MD).
527
528 **Cellular elemental analysis.** Six individual 10 L cultures of HIMB114 were grown in batch for
529 the purpose of collecting 20 L of cultured cells onto triplicate Advantec GF-75, 25 mm diameter
530 glass fiber filters (Sterlitech, Kent, WA, USA), with a nominal pore size of 0.3 µm, for
531 subsequent measurements of cellular C and N quotas. Filters were dried, pelleted, and analyzed
532 using an elemental analyzer (CE440 elemental analyzer, Exeter Analytical, North Chelmsford,
533 MA, USA). The batch cultures were filtered by slowly pumping the cultures from 10 L carboys
534 into large volume filter towers containing combusted 25 mm GF-75 filters; the filtrate was

535 retained in separate 10 L collection carboys for subsequent microscopic analyses to assess the
536 cellular retention efficiency of the filters. A total volume of 30 L was filtered through each
537 membrane filter: 20 L from two separate 10 L cultures, and 10 L of culture filtrate containing
538 cells that passed through the first filtration. The cell retention efficiencies of the filters declined
539 in each successive 10 L round, from a mean retention of 37% in the first round, down to 9% in
540 the final third round of filtration from the filtrate. The overall cell retention rate for the full
541 filtration procedure was 40%, resulting in an average of $5 \pm 2 \times 10^9$ cells (mean ± s.d.; n=3) on
542 each filter. Preliminary tests indicated that procedural blanks were necessary to account for
543 adsorption of non-cellular dissolved C and N onto the filter (Suppl. Info.).

544 For the determination of cellular P, 4 to 5 L of culture were collected by peristaltic pump
545 filtration at a flow rate of 8 mL min^{-1} onto 0.2 µm pore-size, 47 mm diameter PC Nuclepore
546 filters. All filtrations occurred in a walk-in cold room at 4 °C for 8 to 10 h. Procedural blanks of
547 spent media were also made by filtering 50 mL of 0.2 µm media filtrate, that is, the same media
548 in which the cultures were grown with cells removed, onto the 0.2 µm, 47 mm-diameter PC
549 filters. Following filtration, filters were placed in acid-cleaned glass test tubes, covered with
550 combusted aluminum foil and stored at -20 °C until analysis. Cellular P was quantified by a
551 modification of the high temperature combustion, colorimetric molybdate method (46) (Suppl.
552 Info.).

553

554 **Acknowledgements**

555 We thank E. Omori and K. Manoi for laboratory assistance, the laboratory of Craig
556 Carlson at the University of California, Santa Barbara for TOC measurements, and D. Karl for
557 early review and feedback on this research. Nutrient samples were analyzed by the SOEST
558 Analytical laboratory at the University of Hawaii at Manoa. This research was supported by
559 funding from National Science Foundation grant OCE-1538628 to MSR and the Center for
560 Microbial Oceanography: Research and Education (C-MORE, NSF Science and Technology
561 Center award EF-0424599). SF was funded by a C-MORE fellowship. This is SOEST
562 contribution xxxx and HIMB contribution xxxx.

563

564

565 **References**

566 1. Giovannoni SJ. 2017. SAR11 bacteria: The most abundant plankton in the oceans. Ann
567 Rev Mar Sci 9:231–255.
568
569 2. Rappé MS, Connon SA, Vergin KL, Giovannoni SJ. 2002. Cultivation of the ubiquitous
570 SAR11 marine bacterioplankton clade. Nature 2012:630–633.
571
572 3. Zhao X, Schwartz CL, Pierson J, Giovannoni SJ, McIntosh JR, Nicastro D. 2017. Three-
573 dimensional structure of the ultraoligotrophic marine bacterium "*Candidatus* Pelagibacter
574 ubique". Appl Environ Microbiol 83:e02807–16.
575
576 4. Steindler L, Schwalbach MS, Smith DP, Chan F, Giovannoni SJ. 2011. Energy starved
577 *Candidatus* Pelagibacter ubique substitutes light-mediated ATP production for endogenous
578 carbon respiration. PLoS ONE 6:e19725.
579
580 5. Carini P, Steindler L, Beszteri S, Giovannoni SJ. 2013. Nutrient requirements for growth of
581 the extreme oligotroph '*Candidatus* Pelagibacter ubique' HTCC1062 on a defined medium.
582 ISME J 7:592–602.
583
584 6. Raven JA. 1998. The twelfth Tansley Lecture. Small is beautiful: the picophytoplankton.
585 Funct Ecol 12:503–513.
586

587 7. Tripp HJ, Kitner JB, Schwalbach MS, Dacey JWH, Wilhelm LJ, Giovannoni SJ. 2008.
588 SAR11 marine bacteria require exogenous reduced sulphur for growth. Nature 452:741–
589 744.
590
591 8. Tripp HJ, Schwalbach MS, Meyer MM, Kitner JB, Breaker RR, Giovannoni SJ. 2009.
592 Unique glycine-activated riboswitch linked to glycine-serine auxotrophy in SAR11.
593 Environ Microbiol 11:230–238.
594
595 9. Schwalbach MS, Tripp HJ, Steindler L, Smith DP, Giovannoni SJ. 2010. The presence of
596 the glycolysis operon in SAR11 genomes is positively correlated with ocean productivity.
597 Environ Microbiol 12:490–500.
598
599 10. Sun J, Steindler L, Thrash JC, Halsey KH, Smith DP, Carter AE, Landry ZC, Giovannoni
600 SJ. 2011. One carbon metabolism in SAR11 pelagic marine bacteria. PLoS ONE 6:e23973.
601
602 11. Carini P, Campbell EO, Morré J, Sañudo-Wilhelmy SA, Thrash JC, Bennett SE,
603 Temperton B, Begley T, Giovannoni SJ. 2014. Discovery of a SAR11 growth requirement
604 for thiamin's pyrimidine precursor and its distribution in the Sargasso Sea. ISME J 8:1727–
605 1738.
606
607 12. Carini P, White AE, Campbell EO, Giovannoni SJ. 2014. Methane production by
608 phosphate-starved SAR11 chemoheterotrophic marine bacteria. Nature Comm 5:4346.
609

610 13. Dyhrman ST, Ammerman JW, Van Mooy BAS. 2007. Microbes and the marine
611 phosphorus cycle. Oceanogr 20:110-116.
612
613 14. Karl DM 2014. Microbially mediated transformations of phosphorus in the sea: new views
614 of an old cycle. Ann Rev Mar Sci 6:279–337.
615
616 15. Rusch DB, Halpern AL, Sutton G, Heidelberg KB, Williamson S, Yooseph S, Wu D, Eisen
617 JA, Hoffman JM, Remington K, Beeson K, Tran B, Smith H, Baden-Tillson H, Stewart C,
618 Thorpe J, Freeman J, Andrews-Pfannkoch C, Venter JE, Li K, Kravitz S, Heidelberg JF,
619 Utterback T, Rogers Y-H, Falcón LI, Souza V, Bonilla-Rosso G, Eguiarte LE, Karl DM,
620 Sathyendranath S, Platt T, Bermingham E, Gallardo V, Tamayo-Castillo G, Ferrari MR,
621 Strausberg RL, Nealson K, Friedman R, Frazier M, Venter JC. 2007. The Sorcerer II
622 Global Ocean Sampling Expedition: Northwest Atlantic through Eastern Tropical Pacific.
623 PLoS Biol 5:e77.
624
625 16. Martiny AC, Coleman ML, Chisholm SW. 2006. Phosphate acquisition genes in
626 *Prochlorococcus* ecotypes: evidence for genome-wide adaptation. Proc Natl Acad Sci USA
627 103:12552–12557.
628
629 17. Coleman ML, Chisholm SW. 2010. Ecosystem-specific selection pressures revealed
630 through comparative population genomics. Proc Natl Acad Sci USA 107:18634–18639.
631

632 18. Grant SR, Bienfang PK, Laws EA. 2013. Steady-state bioassay approach applied to
633 phosphorus-limited continuous cultures: A growth study of the marine chlorophyte
634 *Dunaliella salina*. Limnol Oceanogr 58:314–324.
635
636 19. Grote J, Thrash JC, Huggett MJ, Landry ZC, Carini P, Giovannoni SJ, Rappé MS. 2012.
637 Streamlining and core genome conservation among highly divergent members of the
638 SAR11 clade. mBio 3:e00252–12.
639
640 20. Karl DM, Björkman KM. 2002. Dynamics of DOP, p 249–366. *In* Hansell DA, Carlson CA
641 (ed), Biogeochemistry of marine dissolved organic matter. Elsevier Science.
642
643 21. Kolowith LC, Ingall ED, Benner R. 2001. Composition and cycling of marine organic
644 phosphorus. Limnol Oceanogr 46:309–320.
645
646 22. Karl DM, Beversdorf L, Björkman KM, Church MJ, Martinez A, DeLong EF. 2008.
647 Aerobic production of methane in the sea. Nat Geosci 1:473-478.
648
649 23. Luo H, Zhang H, Long RA, Benner R. 2011. Depth distributions of alkaline phosphatase
650 and phosphonate utilization genes in the North Pacific Subtropical Gyre. Aquat Microb
651 Ecol 62:61-69.
652

653 24. Villarreal-Chiu JF, Quinn JP, McGrath JW. 2012. The genes and enzymes of phosphonate
654 metabolism by bacteria, and their distribution in the marine environment. Front Microbiol
655 3:19.
656
657 25. Chin JP, Quinn JP, McGrath JW. 2018. Phosphate insensitive aminophosphonate
658 mineralisation within oceanic nutrient cycles. ISME J 12:973-980.
659
660 26. Gundersen K, Heldal M, Norland S, Purdie DA, Knap AH. 2002. Elemental C, N, and P
661 cell content of individual bacteria collected at the Bermuda Atlantic Time-Series Study
662 (BATS) site. Limnol Oceanogr 47:1525–1530.
663
664 27. Makino W, Cotner JB, Sterner RW, Elser JJ. 2003. Are bacteria more like plants or
665 animals? Growth rate and resource dependence of bacterial C:N:P stoichiometry. Funct
666 Ecol 17:121–130.
667
668 28. Van Mooy BAS, Fredricks HF, Pedler BE, Dyhrman ST, Karl DM, Koblizek M, Lomas
669 MW, Mincer TJ, Moore LR, Moutin T, Rappé MS, Webb EA. 2009. Phytoplankton in the
670 ocean use non-phosphorus lipids in response to phosphorus scarcity. Nature 458:69–72.
671
672 29. Kemp PF, Lee S, LaRoche J. 1993. Estimating the growth-rate of slowly growing marine-
673 bacteria from RNA-content. Appl Environ Microbiol 59:2594–2601.
674

675 30. Fagerbakke KM, Heldal M, Norland S. 1996. Content of carbon, nitrogen, oxygen, sulfur
676 and phosphorus in native aquatic and cultured bacteria. Aquat Microb Ecol 10:15–27.
677
678 31. Carini P, Van Mooy BAS, Thrash JC, White A, Zhao Y, Campbell EO, Fredricks HF,
679 Giovannoni SJ. 2015. SAR11 lipid renovation in response to phosphate starvation. Proc
680 Natl Acad Sci USA 112:7767–7772.
681
682 32. Van Mooy BAS, Rocap G, H. F. Fredricks HF, C. T. Evans CT, and A. H. Devol AH.
683 2006. Sulfolipids dramatically decrease phosphorus demand by picocyanobacteria in
684 oligotrophic marine environments. Proc Natl Acad Sci USA 103:8607–8612.
685
686 33. Martiny AC, Vrugt JA, Primeau FW, Lomas MW. 2013. Regional variation in the
687 particulate organic carbon to nitrogen ratio in the surface ocean. Global Biogeochem
688 Cycles 27:723–731 doi: 10.1002/gbc.20061.
689
690 34. Cermak N, Becker JW, Knudsen SM, Chisholm SW, Manalis SR, Polz MF. 2017. Direct
691 single-cell biomass estimates for marine bacteria via Archimedes' principle. ISME J
692 11:825-828.
693
694 35. Church MJ, Ducklow HW, Letelier RM, Karl DM. 2006. Temporal and vertical dynamics
695 in picoplankton photoheterotrophic production in the subtropical North Pacific Ocean.
696 Aquat Microb Ecol 45:41–53.
697

698 36. del Giorgio PA, Condon R, Bouvier T, Longnecker K, Bouvier C, Sherr E, Gasol JM.
699 2011. Coherent patterns in bacterial growth, growth efficiency, and leucine metabolism
700 along a northeastern Pacific inshore-offshore transect. Limnol Oceanogr 56:1–16.
701
702 37. Malmstrom RR, Cottrell MT, Elifantz H, Kirchman DL. 2005. Biomass production and
703 assimilation of dissolved organic matter by SAR11 bacteria in the Northwest Atlantic
704 Ocean. Appl Environ Microbiol 71:2979–2986.
705
706 38. del Giorgio P, Cole J. 2000. Bacterial energetics and growth efficiency, p 289-325. *In*
707 Kirchman D (ed), Microbial Ecology of the Oceans. Wiley-Liss.
708
709 39. Simon M, Azam F. 1989. Protein-content and protein-synthesis rates of planktonic marine-
710 bacteria. Mar Ecol Prog Ser 51:201–213.
711
712 40. Henson MW, Pitre DM, Weckhorst JL, Lanclos VC, Webber AT, Thrash JC. 2016.
713 Artificial seawater media facilitate cultivating members of the microbial majority from the
714 Gulf of Mexico. mSphere 1:e00028–16.
715
716 41. Brandon M. 2006. High-throughput isolation of pelagic marine bacteria from the coastal
717 subtropical Pacific Ocean. MS Thesis. University of Hawaii at Manoa.
718

719 42. Thrash JC, Boyd A, Huggett MJ, Grote J, Carini P, Yoder RJ, Robbertse B, Spatafora JW,
720 Rappé MS, Giovannoni SJ. 2011. Phylogenomic evidence for a common ancestor of
721 mitochondria and the SAR11 clade. Sci Rep 1:1–9.
722
723 43. Parks DH, Chuvochina M, Waite DW, Rinke C, Skarshewski A, Chaumeil PA, Hugenholtz
724 P. 2018. A proposal for a standardized bacterial taxonomy based on genome phylogeny.
725 bioRxiv 256800.
726
727 44. Smith DC, Azam F. 1992. A simple, economical method for measuring bacterial protein
728 synthesis rates in seawater using tritiated-leucine. Mar Microb Food Webs 6:107–114.
729
730 45. Ferrón S, del Valle DA, Björkman KM, Quay PD, Church, MJ, Karl DM. 2016.
731 Application of membrane inlet mass spectrometry to measure aquatic gross primary
732 production by the ^{18}O *in vitro* method. Limnol Oceanogr Methods 14:610-622.
733
734 46. Solorzano L, Sharp JH. 1980. Determination of total dissolved phosphorus and particulate
735 phosphorus in natural-waters. Limnol Oceanogr 25:754–757.
736

737 **Figure Legends**

738 Figure 1. Scanning electron micrographs of HIMB114 cells growing in early stationary phase
739 batch culture. The scale bar corresponds to 1 μm.

740

741 Figure 2. Rates of PO_4^{3-} uptake by SAR11 strain HIMB114. (A) Time course measurements of
742 ^{33}P-phosphate uptake in a chemostat culture of HIMB114 (upper) as well as a batch culture
743 (lower) with blank controls (circles). Solid lines indicate the linear least squares regression,
744 while dashed lines indicate the 95% prediction confidence bands. (B) ^{33}P-phosphate uptake
745 kinetics for a chemostat culture of HIMB114, calculated from single time point, 22-hour
746 incubations across a range of phosphate concentrations.

747

748 Figure 3. Production and respiration of strain HIMB114 during growth in batch culture. (A)
749 Cellular growth (filled circles), bacterial production (^{3}H-Leu; open squares), and dissolved
750 oxygen concentrations (open diamonds) for a 10 L batch culture of HIMB114 measured
751 throughout late exponential and into stationary phase (Table 2, experiment 1). (B) Bacterial
752 production, expressed as molecules leucine per cell per hour over two-hour incubations, vs. daily
753 specific growth rates for the same batch cultures of strain HIMB114, calculated by changes in
754 cell densities between cultures sampled one day apart. The slope of the fit line between
755 production and daily specific growth rate is 0.8 ± 0.3 (95% C.I.) $\times 10^6$ molecules Leu cell^{-1}.

756

757 Figure 4. Respiration of strain HIMB114 during growth in batch culture. (A) Two oxygen
758 respiration incubation experiments (experiments 2 and 3) started from a 10 L batch culture of
759 strain HIMB114 during late exponential phase of growth. (B) Triangles and diamonds represent

760 the mean oxygen concentration for each time point in the second and third incubation
761 experiment, respectively (Table 2, experiments 2 & 3). Error bars represent the standard
762 deviation.
763
764 Figure 5. Chemostat continuous culture of SAR11 strain HIMB114. HIMB114 cells growing at
765 0.3 d^{-1} in chemostat continuous culture in natural seawater media at 26 °C. Standard deviation of
766 cell counts are indicated by error bars. The grey box indicates the time when filling the
767 chemostat, while dotted lines indicate when media in-flow started and new 10 L media reservoirs
768 were connected.
769

770

771

772 Table 1. Mean (± standard deviation), minimum, and maximum bacterial production rates for
773 SAR11 strain HIMB114 grown on sterilized K-bay seawater medium. Production (n=20) was
774 measured in both batch and chemostat cultures by ^{3}H-Leucine incorporation and converted to C
775 units with a leucine to C conversion factor of 1.5 kg C mol Leu^{-1}.

	pmol Leu L^{-1} h^{-1}	amol Leu cell^{-1} h^{-1}	µg C L^{-1} d^{-1}	fmol C cell^{-1} d^{-1}
Mean	16 ±6.5	0.04 ±0.02	0.6 ±0.2	0.13 ±0.07
Max	28	0.1	1.0	0.29
Min	5	0.01	0.2	0.03

776

777

Table 2. Summary of experiments to measure respiration by the time dependent consumption of dissolved O_2 in late-log phase batch cultures SAR11 strain HIMB114. Growth rates were calculated by linear least squares regression of cell density over the 2-day incubation periods. Note that Experiment 1 was conducted toward the transition out of log-phase and into stationary phase growth, with an associated flattening growth curve. Respiration was measured by linear least squares regression of Oxygen concentration with time over the 2-day incubations. Bacterial production values are 2-day means of daily, 2-hour Leucine incubations. Bacterial growth efficiency (BGE) was calculated as described in the text, assuming a respiratory quotient of 1 mol C: mol O_2.

	Growth rate	Abundance	Respiration		Production		BGE
Exp.	Slope ±s.e. (d^{-1})	Mean [min, max] x10^8 cells L^{-1}	Mean [min, max] µmol O_2 L^{-1} d^{-1}	Mean (±95% C.I.) fmol O_2 $cell^{-1}$ d^{-1}	Mean [min, max] µg C L^{-1} d^{-1}	Mean (±95% C.I.) fmol C $cell^{-1}$ d^{-1}	Mean [min, max] (%)
1	0.15 ±0.2	4.0 [3.5, 5.3]	0.36 [0.10, 0.61]	0.90 ±0.65	0.41 [0.30, 0.52]	0.09 ±0.03	9 [5, 26]
2	0.9 ±0.2	3.3 [1.9, 4.8]	0.44 [0.27, 0.60]	1.32 ±0.76	0.82 [0.70, 0.93]	0.27 ±0.06	13 [10, 21]
3	0.5 ±0.1	4.2 [3.3, 4.8]	0.32 [0.14, 0.50]	0.75 ±0.44	0.77 [0.66, 0.87]	0.17 ±0.04	17 [11, 32]

789

790 Table 3. Nutrient concentrations (µmol L^{-1}) for dissolved phosphate (PO_4^{3-}), nitrate plus nitrite
791 ($NO_3^- + NO_2^-$), ammonium (NH_4^+), silicate (SiO_4), total organic C (TOC), and total nitrogen
792 (TN) for natural Kaneohe Bay (K-Bay) seawater with no additions, and the standard SW based
793 medium used to grow HIMB114 in both batch and chemostat cultures.

794

	PO_4^{3-}	$NO_3^- + NO_2^-$	NH_4^+	SiO_4	DOC	TN
K-Bay seawater	0.05	<0.009	0.3	4.3	75	7.5
K-Bay standard medium	0.15	2.4	3.4	4.2	94	13.5

795

796

797

798

799 **Supplemental Material**

800

801 **Supplemental Methods.**

802

803 **Table S1.** Presence of genes for phosphorus uptake and metabolism in selected publicly
804 available SAR11 genomes sequenced from cultivated strains.

805

806 **Figure S1.** Batch culture growth curves for six replicate 10 L cultures of HIMB114. Lower error
807 bars represent the standard deviation among count fields (typically 10-15), while upper error bars
808 represent the cell density if morphologies representing multiple cells are converted to single cell
809 units. The mean regression slope for exponential specific growth rate for the cultures is 1.08 (s.d.
810 0.03) d^{-1}. Strains were grown in using standard media at 26 °C.

811

812 **Figure S2.** Cell size analysis of SAR11 strain HIMB114. Distribution of (A) length, (B) width,
813 and (C) biovolume for N=769 cells, with fit to log-normal distribution.

814

815 **Figure S3.** Filtered media blanks for particulate carbon and nitrogen measurements, as a
816 function of volume of media filtered. Filtered media (47 mm diameter, 0.2 µm pore-size
817 Nuclepore PC membrane followed by 0.22 µm pore-size, Sterivex-GP polyethersulfone
818 membrane) was used as the source for procedural blanks filtered through combusted GF-75
819 glass-fiber filters to correct for adsorption of (A) dissolved organic carbon or (B) inorganic
820 nitrogen. Carbon data fit to a rectangular hyperbolic saturation function: Blank = $8.5(\mu gC) +$

821 $\frac{43.5(\mu gC)\cdot V}{1.9(L)+V}$ for medium volume (V) in liters. Nitrogen data fit to a rectangular hyperbolic

822 saturation function: Blank = $1.1(\mu gN) + \frac{8.1(\mu gN)\cdot V}{2.4(L)+V}$ for medium volume (V) in liters.

823

824 **Figure S4.** Bacterial production versus batch culture growth of strain HIMB114. Bacterial

825 production (measured by ^{3}H-Leu incorporation) during batch culture growth of a single 10 L

826 culture of strain HIMB114, sampled throughout late exponential phase and into stationary phase.

827 Open circles and dotted line indicate cell density, while filled squares and solid line indicate

828 bacterial production.

829

830 **Figure S5.** Volume scaling of the fraction of total cell volume occupied by the genome (solid

831 line) and the cell envelope (dashed line) for a theoretical bacterial cell. Cell size parameters

832 calculated assuming spherical cells, with volume of the cell envelope calculated assuming a

833 spherical shell with an envelope thickness of 20 nm. Genome volume calculated assuming a

834 genome length of 1.237 Mbp, and a DNA volume per base pair of 1 nm^3. At the volume of the

835 most frequent HIMB114 cell (0.05 µm^3), the cell envelope and genome take up 26% and 2.5% of

836 the cell volume, respectively.

837

838 **Figure S6.** Batch growth and nutrient dynamics numerical model results (blue lines) for a batch

839 culture of HIMB114, using phosphate as a sole source of phosphorus. (A) Phosphate (Pi) pool

840 concentration; (B) rate of change of the Pi pool $\left(\frac{dP}{dt}\right)$ due to uptake by cells; (C) Pi pool turnover

841 time (T_P), with gray horizontal solid line indicating the minimum turnover time of 50 d, and gray

842 dashed horizontal line showing when the turnover time is one order of magnitude above the

minimum (500 d); (D) culture biomass as phosphorus concentration, with actual P-biomass calculated from cell counts from the culture (circles); (E) phosphate uptake rate dynamics, assuming phosphate as a sole source of phosphorus. The observed uptake rate value is plotted as a horizontal dashed gray line near the bottom of the y-axis, measured late on day 7 at 0.004% total P d^{-1}. This intersects the modeled rate on day 11.6, nearly four days following the observed rate. (F) Similar to panel C, but with Pi pool turnover time in units of years and on a linear scale. Colored areas indicate time windows for turnover times less than 1 (light blue), 10 (blue), and 50 (purple) years. For all panels, the gray dashed vertical line indicates the time of highest uptake rate of phosphate, or equivalently the shortest turnover time. This corresponds closely to the actual timing of the measured Pi uptake experiments from the HIMB114 batch cultures, shown by the cell density circle closest to the vertical line in panel D.

Figure S7. ^{3}H-Leucine incorporation by HIMB114 as a function of incubation time.

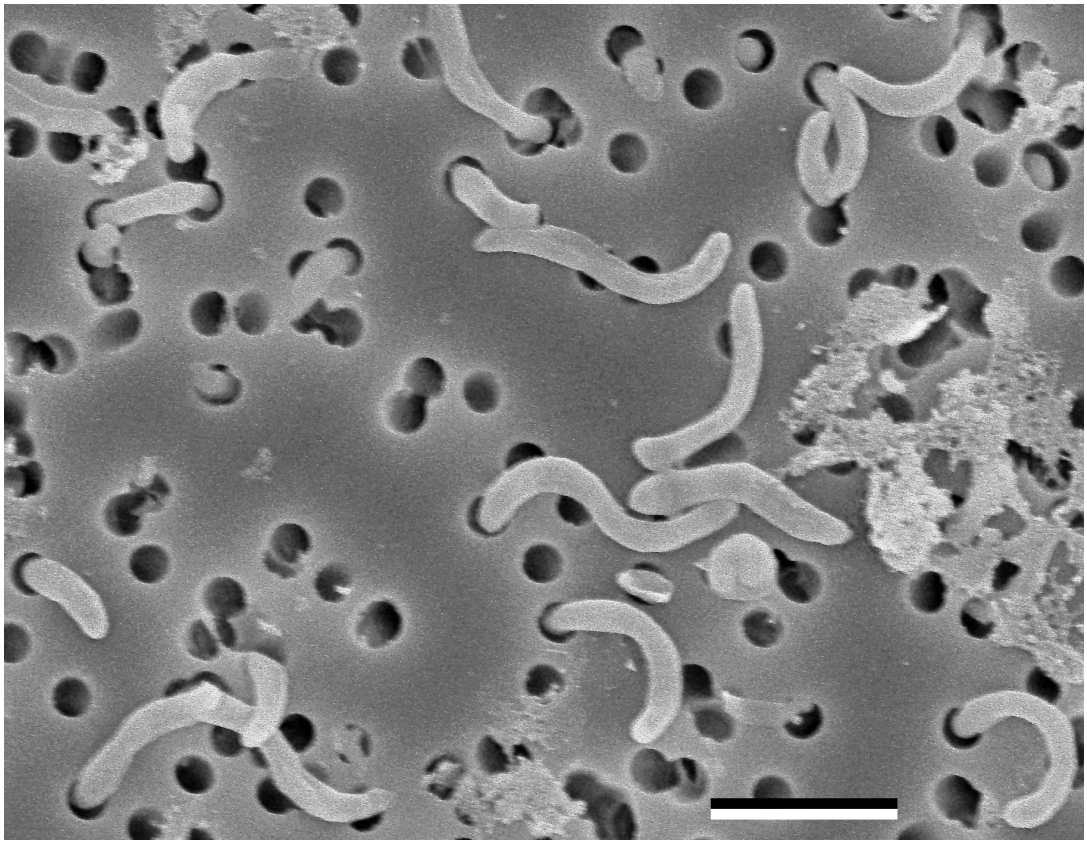

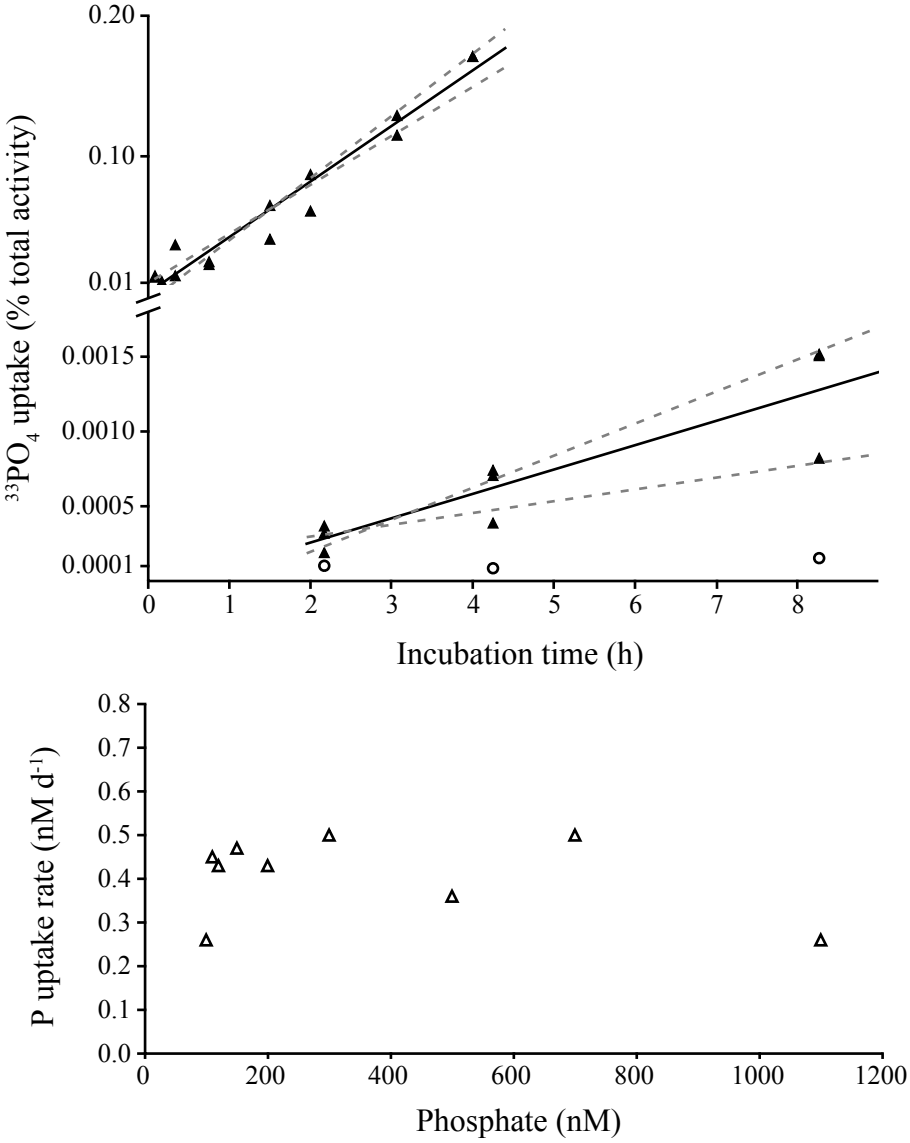

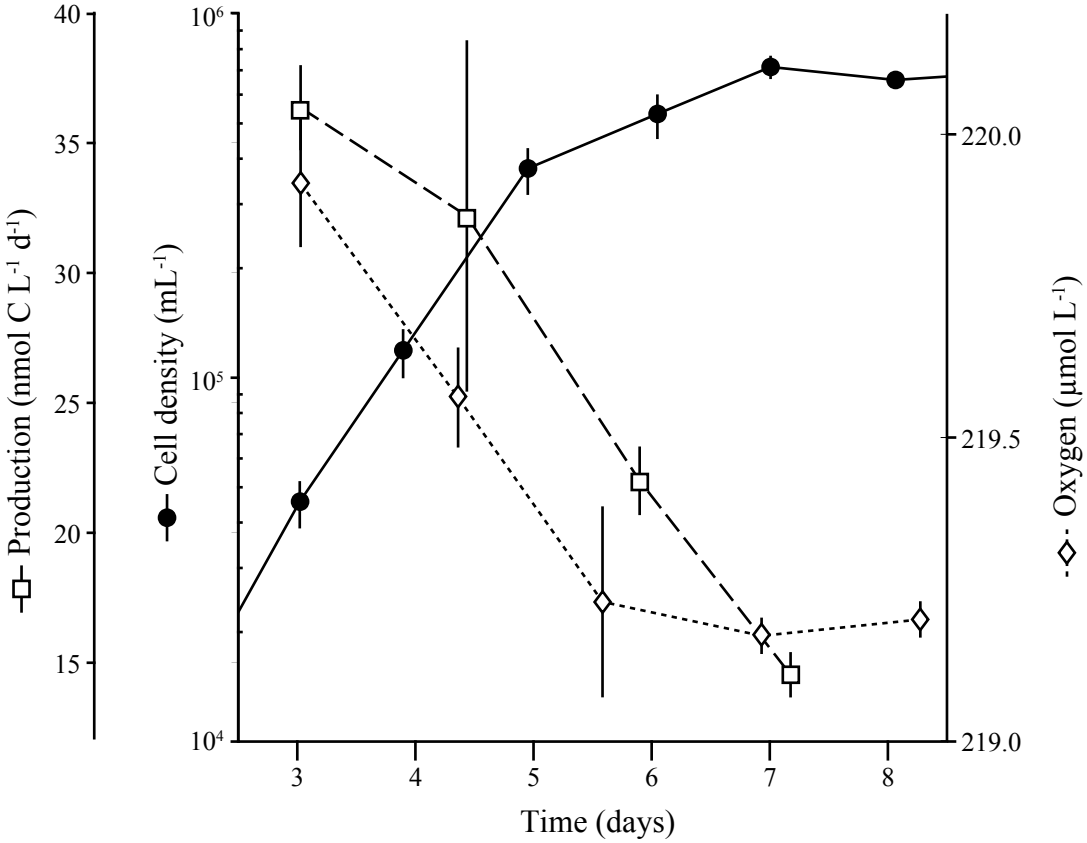

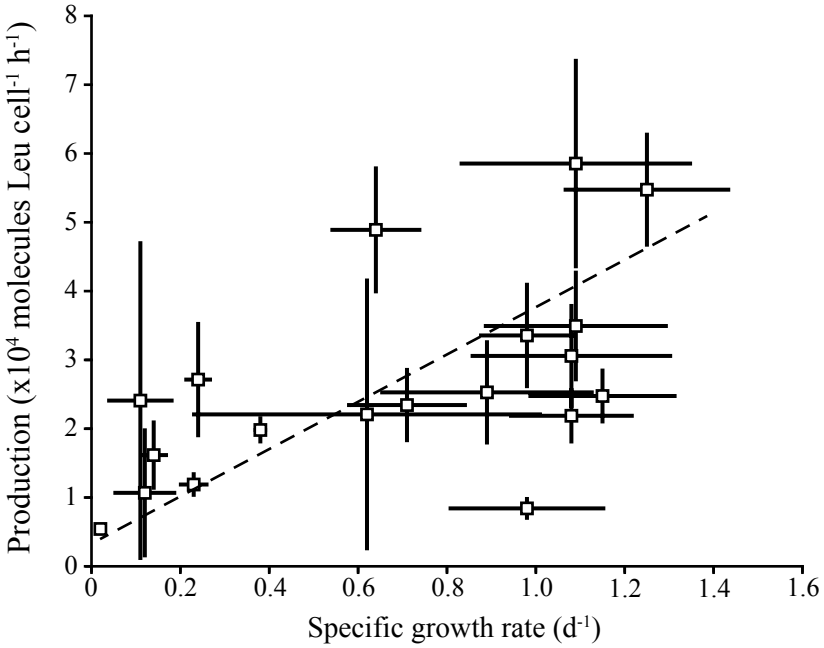

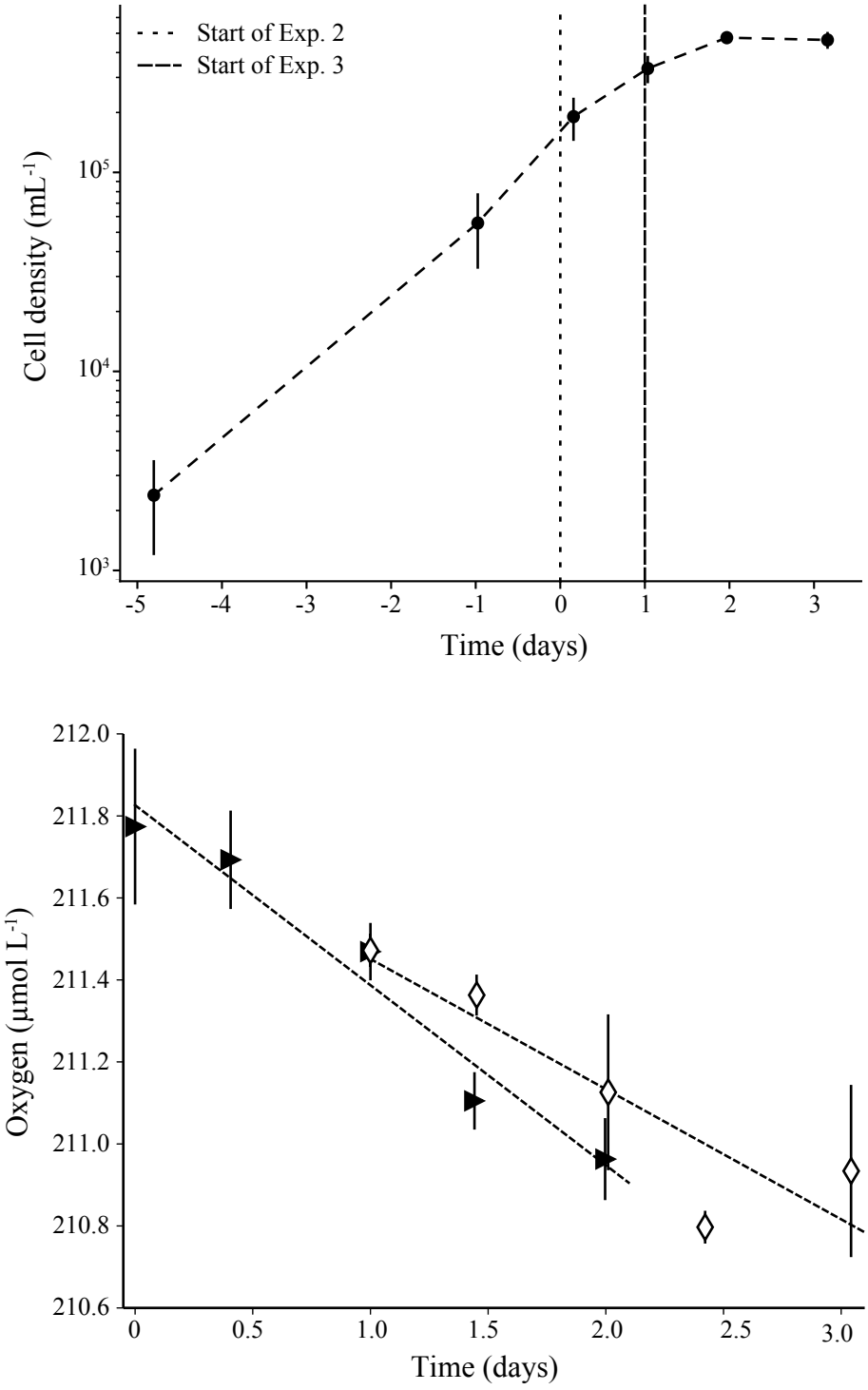

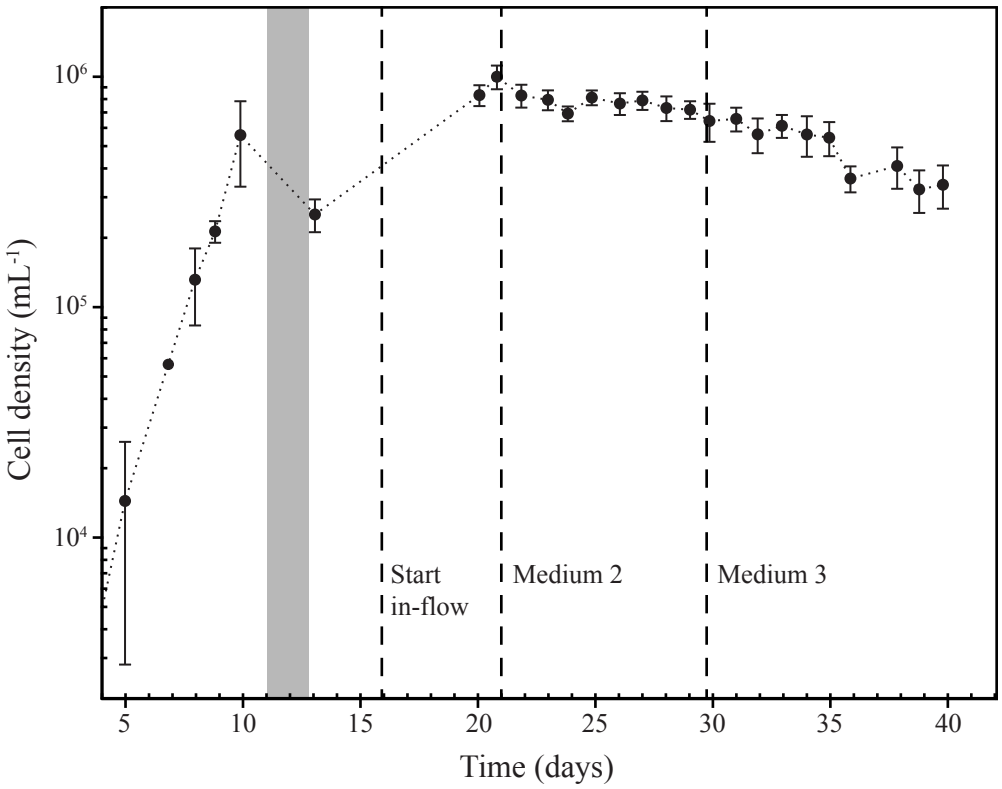

Supplemental Methods

Cell enumeration and image analysis

Cell biovolume (V) was calculated from cell length (L) and width (W) using a bulk geometric function for a prolate spheroid, $V = \frac{\pi}{6} W^2 L$. Although the bulk geometric function for a prolate spheroid has been shown to overestimate volumes for objects with similar shape morphology to HIMB114 by about 50%, it is likely the most appropriate bulk formula to use, and is better than using an equation for a cylinder with hemispherical caps, which can overestimate volumes for these shapes by 100% (Sieracki, Viles, & Webb, 1989).

Phosphate uptake

Control tests were made for the non-biological adsorption of ^{33}P-tracer to both Nuclepore PC and Supor PES membranes (Pall Corp.) with and without the high-phosphate pre-saturation step. PC membranes were found to be superior to PES membranes for lowering control background, retaining just 0.0001% and 0.05% of the total ^{33}P activity with and without the high-phosphate pre-saturation step, respectively. The Supor PES membranes retained significantly more of the ^{33}P-phosphate radiotracer, 0.07% and 0.34% of the total activity with and without the high-phosphate step, and with much higher variance between replicates than for the PC membranes. Therefore, PC membranes were chosen as the preferred filters for reducing both the background and sample variance for ^{33}P-phosphate uptake measurements.

Batch growth and nutrient dynamics model

A numerical model to describe the dynamics of batch culture growth was constructed to provide insights and theoretical comparisons for the measured PO_4^{3-} uptake rates and turnover

times under batch growth conditions. The model is cast in units of P concentration, in order to describe the uptake of PO_4^{3-} and growth of the culture with the assumption that PO_4^{3-} is the sole source of P for the culture.

The prognostic equation for the culture cell density (x) is described by a second order logistic equation:

$$\frac{dx}{dt} = \mu \cdot v \cdot x \cdot \left[1 - \left(\frac{x}{x_{max}}\right)^n\right]$$

where n is the exponential constant for logistic growth, which we set to 2 after investigating the growth curves for n = 1 to 4 (an exponent higher than 1 is needed to correctly model the observed, rapid transition from exponential to stationary phase); x_{max} is the observed maximum cell density for the culture; v is the rectangular hyperbolic Monod function for phosphate limited growth, which never came into effect here because the phosphate pool never approached, within an order of magnitude, the assumed phosphate half-saturation constant for growth of $K\mu$ = 1 nM P. The growth rate function, μ, is used to describe the transition from the lag phase to the exponential maximum growth rate phase, and is also described by a logistic equation:

$$\frac{d\mu}{dt} = \frac{1}{\tau} \cdot \mu \left[1 - \left(\frac{\mu}{\mu_{max}}\right)\right]$$

where τ is the timescale for the lag phase transition to exponential growth (1 d), and μ_{max} is the observed exponential phase growth rate. To convert from cell density to P-based biomass units, the measured P cell quota (Q_P) is assumed to be constant throughout the growth curve, and the

growth of cell biomass is directly coupled to the uptake of P from the phosphate pool:

$$\frac{dp}{dt} = -\frac{dx}{dt} \cdot Q_P$$

with observed initial concentrations of P and x used to initialize the model. The model was stepped forward with a time step of 30 minutes for 12 days using a simple Newton numerical scheme.

Because of the inherent non-linear dynamics of batch growth conditions, the theoretical nutrient uptake rates and turnover time may be quite dynamic, potentially changing by an order of magnitude on a daily timescale, making the interpretation of a measured rate on any particular day difficult. Results from the model matched reasonably well with the observed growth curve, and also confirmed that the time of maximum PO_4^{3-} uptake rates (Fig. S6E) and minimum turnover time (Fig. S6C) occur at the end of the exponential phase of growth (Fig. S6D). This corresponded quite closely to when the PO_4^{3-} uptake measurements were measured on this culture (Fig. S6D). The maximum theoretical specific uptake rate calculated by the model was 2×10^{-2} d^{-1}, or 3 nmol P L^{-1} d^{-1}, compared to the observed specific rate of 4×10^{-5} d^{-1}, or 6 pM P L^{-1} d^{-1}, measured very close to this time. The theoretical uptake rate falls off exponentially on either side of the maximum (Fig. S6E). The model also indicates that the minimum turnover time for the PO_4^{3-} pool, occurring on day 7.8, should be close to 50 days, again increasing exponentially around the minimum. The actual turnover time measured at the end of day 7 was 70 years (range from 50 to 150), about 500 times the minimum turnover time. Even if the lower estimate of 50 years is used, the timing would need to be off by over 3.5 days to measure a turnover time of that scale (Fig. S6).

Knowing what range of PO_4^{3-} turnover times to expect on a theoretical basis is quite difficult in batch cultures because of the non-linear dynamics, for which there is no clearly superior choice of functional parameterization for modeling batch culture growth (Zwietering et al., 1990). This creates a large uncertainty, of likely an order of magnitude, in the modeled uptake rates, which are particularly sensitive to the timing within the growth curve. Nevertheless, the turnover time was measured at what should be quite close to the time in the growth curve that would coincide with the minimum turnover time for PO_4^{3-}, and yet the measured turnover times were at least 500 times larger than expected.

Bacterial production

Typically, quadruplicate 1.5 mL sample volumes and duplicate blanks were added into 2 mL microcentrifuge tubes, followed by 2 µL of ^{3}H-3,-4,-5-Leucine (106 Ci mmol^{-1}; 5 mCi mL^{-1}; PerkinElmer) to a final concentration of 60 nmol Leu L^{-1}, mixed well, and incubated for 2.5 h under the same temperature and light conditions as the original cultures. Blanks were killed with trichloroacetic acid (TCA, 5% final) before the addition of ^{3}H-Leu. Incubations were stopped by the addition of TCA (5% final, 4 °C), centrifuged (14,000 rpm at 4 °C for 15 min), rinsed with 1 mL 5% TCA (4 °C), centrifuged again (14,000 rpm at 4 °C for 5 min), then rinsed with 1 mL 80% ethanol (4 °C) and centrifuged (14,000 rpm at 4 °C for 5 min). Pellets were allowed to dry overnight at room temperature in a fume hood before adding 1 mL of scintillation cocktail (UltimaGold LLT; PerkinElmer), vortexed, and allowed to sit for at least four days before making final activity counts (PerkinElmer Tri-Carb Liquid Scintillation counter), as the activity was observed to increase over the first two days after adding cocktail. Activity counts were converted to leucine concentration based on the specific activity of the isotope and

calibrated to a ^{3}H standard. Prior to using single 2.5-hr time point incubations, the linearity of ^{3}H-Leu incorporation by the HIMB114 culture was tested over 4 h and found to be quite linear over that time period (Fig. S7).

Oxygen respiration

Oxygen concentration measurements were made based on the mass spectrometric determination of the ratio of oxygen to argon. Briefly, the seawater sample was continuously pumped across a permeable membrane under vacuum, allowing dissolved gasses to diffuse across the membrane that were detected by an in-line mass spectrometer. An equilibrated seawater standard was used for calibration, and the oxygen concentration was calculated by the change in the O_2/Ar ratio referenced to the initial, time zero, oxygen concentration. Oxygen respiration rates were then calculated by linear least squares regression of oxygen concentration versus incubation time over two-day periods.

Cellular Elemental Analysis

Carbon and Nitrogen. Preliminary tests of filtration methods indicated that filtration by even the lowest of vacuum pressure retained undetectable cells, while filtration by gravity retained at most 50% of cells. This was slightly better than very slow (5 mL min^{-1}) peristaltic pump filtration, which was comparable to the rate of filtration by gravity. Because of the very slow filtration rates by gravity in combination with the large volumes that needed to be filtered, filtrations were conducted in a 4 °C walk-in cold room in order to stop cellular metabolism, and carried out over a period of 8 days of continuous gravity filtration. Pump speeds were adjusted to keep pace with the gravity filtration rates, which started at 3.5 mL min^{-1} and gradually slowed to

2 mL min^{-1} by day 5. Once filtration rates slowed to below 1 mL min^{-1} (day 8) the filtration was stopped.

For procedural blanks, batch cultures were 0.2 µm-filtered twice to remove all cells (0.2 µm pore-size, 47 mm-diameter Nuclepore PC membrane followed by 0.22 µm pore-size, Sterivex-GP PES membrane) and the filtrate used to construct dissolved carbon and nitrogen blank saturation curves by filtering 0, 1, 2, 5, and 10 L of sterile-filtered media through combusted GF-75 filters. These filters were then analyzed for carbon and nitrogen along with the sample filters (Fig. S3).

Phosphorus. Tubes containing sample filters were combusted for 9 h at 450 °C in order to convert organically bound phosphorus to inorganic phosphate, which was then extracted in 10 mL of 0.15 M HCl for 1 h at room temperature. Sub-samples (5 mL) of the acid extract were reacted with 0.5 mL of a molybdate mixed reagent solution to develop the blue phospho-molybdate complex. The molybdate mixed reagent was made by combining 10 mL of 30 g L^{-1} ammonium paramolybdate solution, 25 mL of 5N sulfuric acid, 10 mL of 5.4 wt.% ascorbic acid solution, and 5 mL of 1.7 g L^{-1} potassium antimony-tartrate solution. After allowing one h for color development, absorbance was measured on a spectrophotometer at 880 nm using a 1 cm path length quartz cell. Phosphorus concentrations were calculated using a phosphate standard curve, with the mean absorbance of the media procedural blanks subtracted from the sample absorbance.

Supplemental References

Sieracki ME, Viles CL, and Webb KL. 1989. Algorithm to estimate cell biovolume using image analyzed microscopy. Cytometry 10:551–557.

Zwietering MH, Jongenburger I, Rombouts FM, Vantriet K. 1990. Modeling of the bacterial-growth curve. Appl Environ Microbiol 56:1875–1881.

Table S1. Presence of genes for phosphorus uptake and metabolism in selected publicly available SAR11 genomes sequenced from cultivated strains.

Strain	Lineage	Source	pstS phosphate transport	phoBU phosphate regulation	phnCDE phosphonate transport	phnAGHI JKLMNX phosphonate metabolism	ppx/ppk polyphosphate metabolism
HIMB114	IIIa	Subtropical North Pacific	+	+	+	phnAX	-
HIMB58	IIb	Subtropical North Pacific	+	+	-	-	-
HIMB59	V	Subtropical North Pacific	+	+	+	phnAX	-
HIMB5	Ia	Subtropical North Pacific	+	+	-	-	-
HTCC7211	Ia	Sargasso Sea, Atlantic	+	+	+	+	+
HTCC9565	Ia	Temperate North Pacific	-	phoH	-	-	-
HTCC1002	Ia	Temperate Coastal Pacific	-	phoH	-	-	-
HTCC1062	Ia	Temperate Coastal Pacific	+	+	-	-	-